

DYNAMIC FRACTURE TOUGHNESS IN CERAMICS AND CERAMICS MATRIX COMPOSITES†

T. KISHI

Research Center for Advanced Science and Technology, The University of Tokyo, 4-6-1 Komaba, Meguro-ku, Tokyo 153, Japan

Abstract—The dynamic fracture toughness K_{I_d} of ceramics and ceramics matrix composite was evaluated both by the strain gage method and by the load deconvolution method over a wide range of loading rates using both conventional Instron-type and the newly developed drop-type impact testing machines, and the result was compared with the two-dimensional dynamic finite element method. Six kinds of ceramics were tested: fine and coarse grained alumina, tetragonal zirconia polycrystal (TZP), silicon carbide, silicon nitride and sialon. Two kinds of SiC whisker and ZrO₂ particle-reinforced Al₂O₃ matrix composites were also tested. Lastly, the effect of operating temperature on dynamic fracture toughness was examined.

INTRODUCTION

UNDER DYNAMIC loading conditions, it is important to evaluate the critical stress intensity factor at fracture initiation, that is, the dynamic fracture toughness K_{I_d} . In this treatment, Wilson *et al.* have reported that the dynamic fracture toughness of certain steel is lower than the corresponding static one when fracture occurs by cleavage[1]. Since ceramics are expected to fracture by quasi-cleavage, it is therefore important to determine whether the dynamic fracture toughness differs from the static one or not.

Abe *et al.*[2] obtained the K_{I_d} of notched SiC specimens by instrumented charpy testing, while Gonczy and Johnson have applied the indented surface flaw technique at elevated temperatures, but their estimated loading rate was about 10^4 MPam^{1/2} s⁻¹[3]. Both Abe *et al.* and Gonczy and Johnson evaluated the K_{I_d} from the maximum load using a static formula. Since their load-time traces exhibited few or no oscillations, their quasi-static treatment may be reasonable, but their maximum loading rate was not so high.

Kobayashi *et al.*[4] have evaluated the K_{I_d} of partially stabilized zirconia (PSZ) and silicon nitride at loading rates higher than 10^5 MPam^{1/2} s⁻¹ using the impact responses curve. They observed a significant increase of K_{I_d} with loading rates between 10^5 and 10^6 MPam^{1/2}, and ascribed this increase to the loading rate dependency of stress-induced transformation and incubation time[5]. However, care should be taken when applying the impact response curve method determined with notched specimens to precracked specimens. The impact response of a precracked specimen is different from that of a notched one because of the apparent residual stress around the precrack.

Thus, the intent of the present paper is to try to establish an experimental method of evaluating K_{I_d} of ceramics at loading rates greater than 10^5 MPam^{1/2} s⁻¹, where quasi-static treatment is no longer possible.

EXPERIMENTAL PROCEDURES

Materials

Six kinds of ceramics were tested, namely coarse grained alumina (ADS10), fine grained alumina (ADS80), tetragonal zirconia polycrystal (TZP), silicon nitride, silicon carbide and sialon. The grain boundaries of Si₃N₄, sialon and SiC were crystallized by heat treatment. The density and mechanical properties of these materials are shown in Table 1 and the specimen sizes in Fig. 1. Also, SiC whisker and ZrO₂ particle-reinforced Al₂O₃ matrix composites were tested. All the specimens were precracked before fracture toughness testing by the bridge indentation technique[6].

†Plenary Paper.

Table 1. Mechanical properties of specimens

Material	Density (g cm ⁻³)	Young's modulus (GPa)	Poisson's ratio	Grain size (μm)
Al ₂ O ₃ (ADS10)	3.85	377	0.231	20
Al ₂ O ₃ (ADS80)	3.57	222	0.235	5
ZrO ₂ (TZP)	6.07	207	0.32	0.5
Si ₃ N ₄	3.23	320	0.27	1
Sialon	3.25	301	0.28	—
SiC	3.13	398	0.17	—

Al₂O₃ + 20 wt% SiC + 10 wt% ZrO₂.
Al₂O₃ + 20 wt% SiC + 20 wt% ZrO₂.

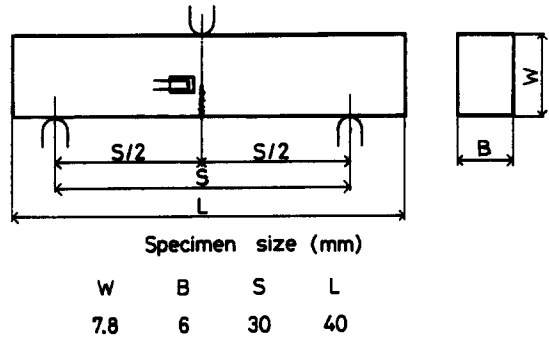


Fig. 1. Specimen size used in dynamic testing.

Testing

A drop weight impact testing machine was newly developed for this experiment. Impact velocities up to 1 m s⁻¹ were controlled by a pulley system, and above 1 m s⁻¹ they were controlled by manual lifting to a predetermined height. Static fracture toughness testing was carried out using a conventional Instron type instrument. Cross-head speeds were varied from 0.005 mm min⁻¹ to 200 mm min⁻¹.

Methods for determining dynamic fracture toughness

The dynamic stress intensity was evaluated both by the strain gage method and by the deconvolution method. A strain gage attached near the crack tip was calibrated by static loading, and the relation between strain and static stress intensity was obtained from the ASTM E399 standard. A typical strain-load calibration curve is shown in Fig. 2. Though a non-linearity appeared in the lower K_I range, linear behavior is observed in the higher K_I range. The dynamic fracture toughness was evaluated from the maximum point of the specimen strain signal using this strain- K_I calibration curve under the assumption that the fracture initiated at that point. Also, numerical simulations were carried out using the two-dimensional dynamic finite element method, which was developed by Kanto and Yagawa[7]. The strain- K_I relation was obtained in both static and dynamic cases, and it illustrates that the strain- K_I relations are almost the same in both the static and dynamic cases, as shown in Fig. 3. From this result it can be concluded that the strain gage method is applicable to evaluate dynamic stress intensity factors.

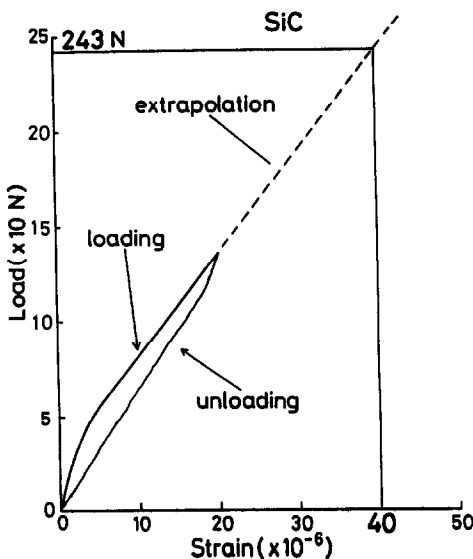


Fig. 2. Load-strain gage calibration curve.

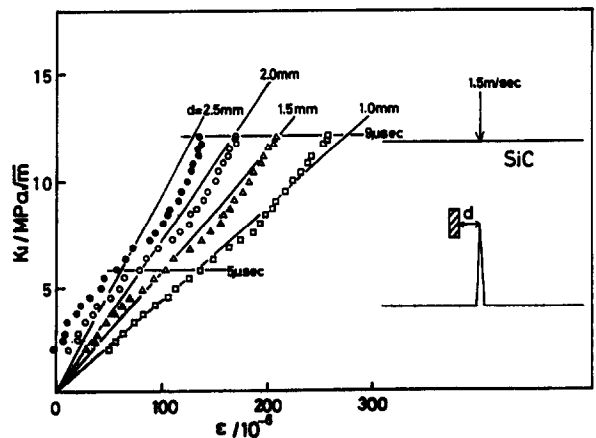


Fig. 3. Dynamic and static stress intensity (solid line) as functions of relative distance between crack tip and strain gage position.

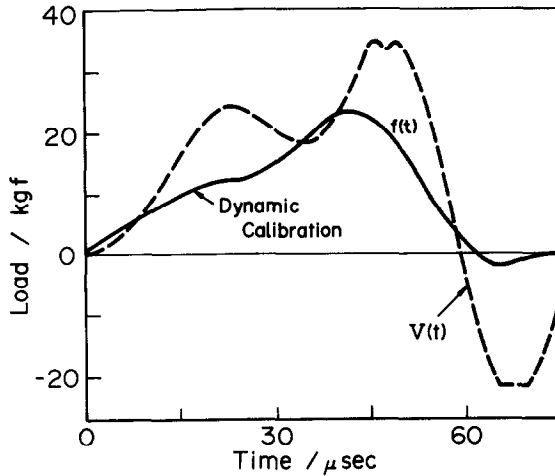


Fig. 4. Detected signal $V(t)$ and deconvoluted dynamic calibration curve $f(t)$.

The strain gage method is not valid at elevated temperatures, so we also developed a deconvolution method. The output signal $V(t)$ of the strain gage at the top of a dropping ball can be formulated by

$$V(t) = h(t) \otimes f(t)$$

where $h(t)$ is a dynamic Green function indicating impacted stress wave propagation, $f(t)$ is the actual load at the impacted specimen surface and \otimes shows the convolution integral. It is well known that $h(t)$ can be obtained experimentally by using a standard impact signal such as breaking pencil lead[8]. So by carrying out the deconvolution integral, we can obtain the actual loading $f(t)$ at the impact point from the initial detected signal $v(t)$, as shown in Fig. 4. Since the maximum load of $f(t)$ corresponds to the maximum strain of the strain gage at crack tip, it is expected that this maximum load corresponds to crack initiation. From this result it can be concluded that the deconvolution method is an excellent method for obtaining the dynamic fracture toughness at elevated temperatures.

RESULTS

Figure 5 shows the obtained results of dynamic fracture toughness in Si_3N_4 , and it is clear that both strain gage and deconvolution methods give the same results. Here the strain gage method was applied to obtain K_{Iid} at room temperature and the deconvolution method was used at elevated temperature.

Figure 6 shows the loading rate dependency of K_{Iid} in Al_2O_3 . The fracture toughness of coarse grained alumina increased from 5 to 10 $\text{MPa}\sqrt{\text{m}}^{1/2}$ with the loading rate exceeding $5 \text{ MPa}\sqrt{\text{m}}^{1/2} \text{ s}^{-1}$.

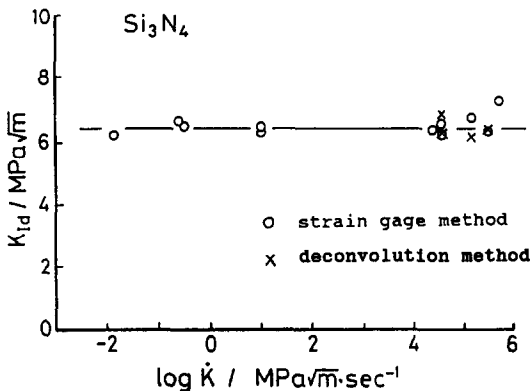


Fig. 5. Loading rate dependence of fracture toughness for Si_3N_4 .

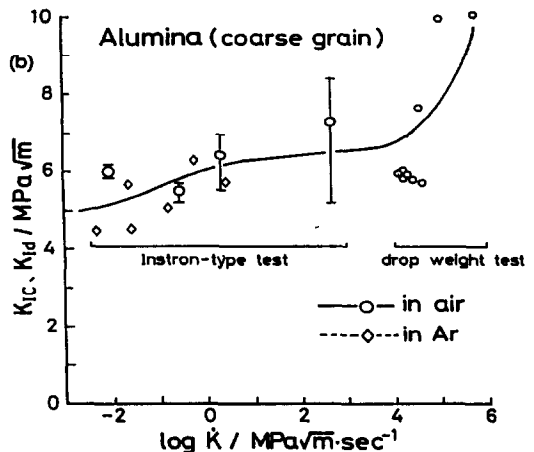


Fig. 6. Loading rate dependence of fracture toughness K_{Iid} of coarse grained Al_2O_3 .

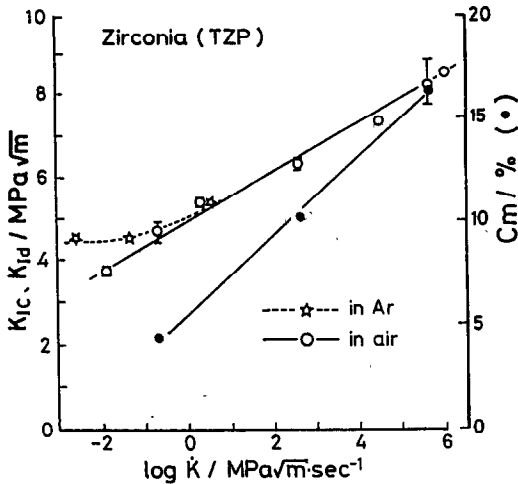


Fig. 7. Fracture toughness K_{Ia} and transformed ratio C_m as a function of loading rate \dot{K} .

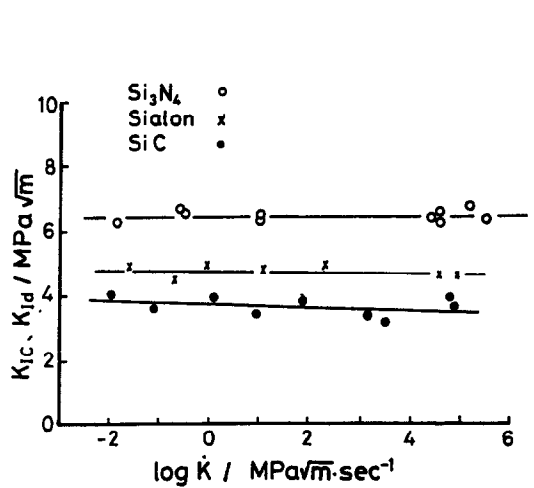


Fig. 8. Loading rate dependence of fracture toughness in SiC, sialon and Si_3N_4 .

The K_{Ia} of fine grained alumina also showed almost the same dependency but increased from 4 to 7 $MPa\sqrt{m}$. For the purpose of studying the effect of humidity of the atmosphere, testing in an Ar atmosphere was also carried out and no significant effect was observed.

Figure 7 illustrates the loading rate dependency of fracture toughness of TZP, which increased monotonically from 3.6 to 8 $MPa\sqrt{m}$. Experiments in an Ar atmosphere showed less loading rate dependency, as loading rates ranging from -2 to 1 $MPa\sqrt{m} s^{-1}$ were observed.

The fracture toughness of SiC, Si_3N_4 and sialon remained almost constant, as shown in Fig. 8.

SiC whisker and particle-reinforced Al_2O_3 composites showed slightly increased results at higher loading rates, as shown in Fig. 9. This will become a remarkable point in composite. Figure 10 shows a temperature dependence of the fracture toughness of Al_2O_3 . K_{Ia} decreases slightly with increasing temperature.

DISCUSSION

The K_{Ia} of Al_2O_3 and TZP increased with increasing \dot{K} ($=dK/dt$), while the K_{Ia} in SiC, Si_3N_4 and sialon remained almost constant. The K_{Ia} of TZP in an Ar atmosphere showed no dependency at the lower range of \dot{K} and a higher value than the corresponding one in air. This is because the loading rate dependency at lower loading rate in air was caused by the results which coincide with the observations of the fractography shown in Fig. 11. The fractographic features of slow crack growth are observed in the region between precrack and fast crack growth. The width of the slow crack growth region decreased with increasing \dot{K} , and remained almost the same in the higher \dot{K}

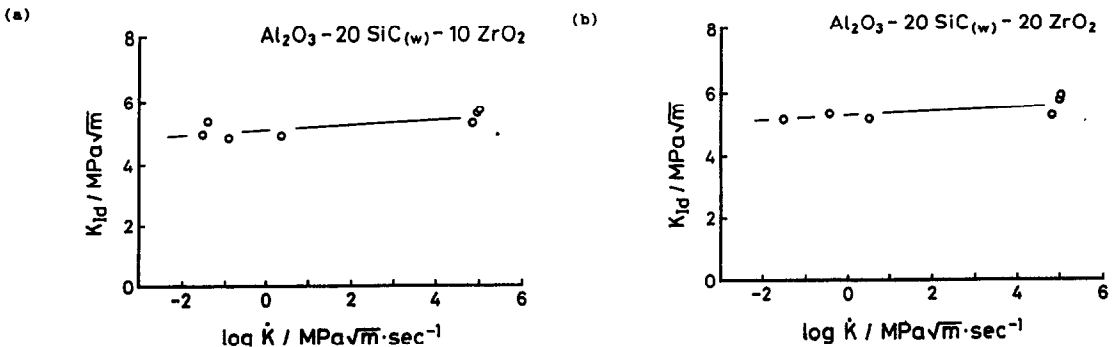


Fig. 9. Loading rate dependence of fracture toughness for $Al_2O_3-20\% SiC-10\% ZrO_2$ (a) and $Al_2O_3-20\% SiC-20\% ZrO_2$ (b).

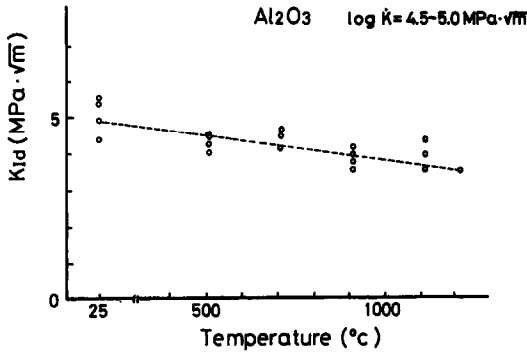


Fig. 10. Temperature dependence of dynamic fracture toughness of Al_2O_3 .

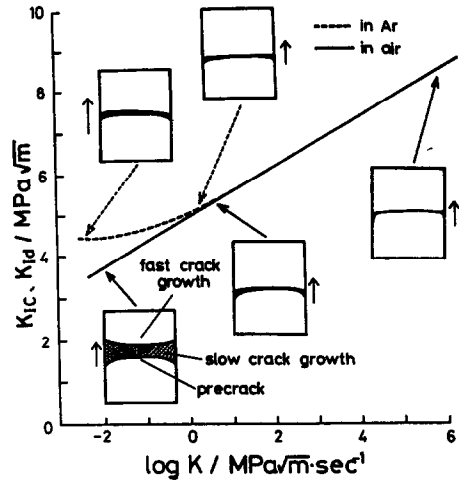


Fig. 11. Variation of the hatched width of slow crack growth as a function of loading rate.

range. However, the increase of K_{Id} at higher \dot{K} may be explained by the stress-induced martensitic transformation from the tetragonal to the monoclinic phase as follows.

In order to investigate the relation between the amount of transformation and K_{Id} , measurements of the fraction of transformed monoclinic phase were carried out by Raman microprobe analysis. An example of a spectrum is shown in Fig. 12, measured at a point 0.1 mm distant from the precrack tip in the direction of crack propagation. The monoclinic fraction (C_m) was calculated from the following equation:

$$C_m = \frac{I_m^{181} + I_m^{192}}{(I_t^{148} + I_t^{265}) + (I_m^{181} + I_m^{192})}$$

where t and m identify the integrated intensity of the Raman peak of the tetragonal and monoclinic phases, respectively, and the number is the Raman shift in C_m^{-1} .

In Fig. 7 the relation between calculated monoclinic fraction and loading rate is also represented. The loading rate dependency of K_{Id} may be interpreted as the result of the transformation. It is well known that stress-induced transformation plays an important role for toughening in Zirconia ceramics, but it may also be possible to regard inversely the loading rate dependency of the transformation as the result of the increase of K_{Id} at higher loading rate. Further efforts are needed in this regard.

Since no apparent differences in fracture appearances for Al_2O_3 were observed by SEM fractographs, the incubation time theory of Kalthoff[9] might explain the significant increase in K_{Id} at loading rates higher than $10^5 \text{ MPa m}^{1/2} \text{ s}^{-1}$. Incubation time theory states that, for unstable fracture to occur, $K_I(t)$ must exceed K_{Id} for some minimum time. It has often been cited that microcracking plays a very important role in the fracture mechanism of Al_2O_3 ceramics[10]. Kishi

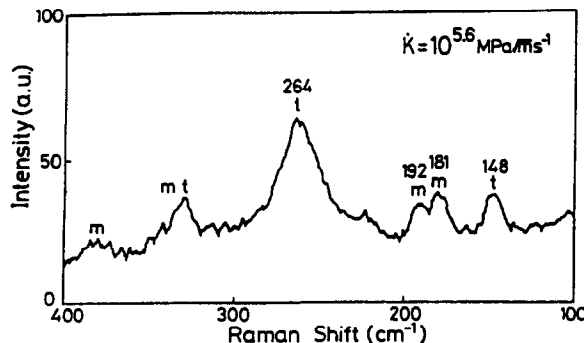


Fig. 12. An example of a Raman spectrum at the crack tip of TZP.

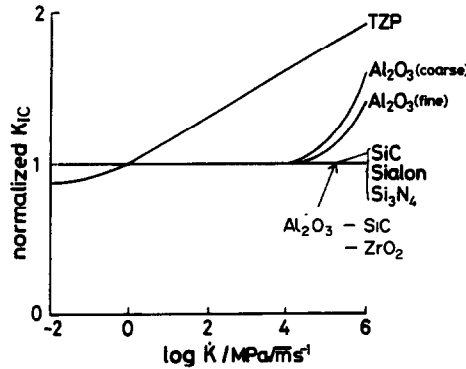


Fig. 13. Normalized fracture toughness of ceramics and ceramics matrix composites as a function of loading rate.

et al. have shown that the time required for microcrack nucleation is 0.1–0.9 μs in Al_2O_3 [5]. Therefore it is quite reasonable to consider that some minimum time is required for these microcracks to build up to a critical state. However, it should be noted here that the K_{Ic} of Al_2O_3 containing a large amount of glassy phase depended a great deal on the loading rate, while those of SiC, Si_3N_4 and sialon, containing no glassy phase, showed little dependency. It might be suspected that the intergranular glassy phase delayed fracture initiation under dynamic loading conditions due to a viscoelastic effect. This discussion shows that much research work is necessary in this field.

Figure 13 shows the normalized loading rate dependency of K_{Ic} of these ceramics. Lastly, temperature dependence can be explained by temperature dependence of the modules.

CONCLUSIONS

1. Dynamic fracture toughnesses of ceramics were evaluated by the strain gage method at room temperature in the loading rate range up to $10^6 \text{ MPam}^{1/2} \text{ s}^{-1}$. The method was verified by the dynamic finite element method.

2. The deconvolution method of detected strain gage signal was also developed to obtain dynamic fracture toughnesses at elevated temperatures.

3. The fracture toughnesses of alumina and TZP increased with loading rate, while those of sialon, Si_3N_4 and SiC remained almost constant. In the case of TZP, the increase of K_{Ic} in the lower \dot{K} range was found to be caused by humidity in the ambient atmosphere, and in the higher \dot{K} range the increase was ascribed to the amount of transformation.

4. In SiC whisker and ZrO_2 particle-reinforced Al_2O_3 composites, the dynamic fracture toughness increased slightly compared with the static value.

5. Dynamic fracture toughness decreases with increasing operating temperature in Al_2O_3 and Si_3N_4 .

REFERENCES

- [1] M. L. Wilson, R. H. Hawley and J. Duffy, *Engng Fracture Mech.* **13**, 371 (1980).
- [2] H. Abe, H. C. Chandan and R. C. Bradt, *Am. Ceram. Soc.* **57**, 589 (1978).
- [3] S. T. Gonczy and D. L. Johnson, in *Fracture Mechanics of Ceramics* (Edited by R. C. Bradt, D. P. H. Hasselman and F. F. Lange), Vol. 3, p. 495. Plenum Press, New York (1978).
- [4] T. Kobayashi, K. Matsunuma, H. Ikawa and K. Motoyoshi, *J. Jap. Inst. Metals* **51**, 723 (1987).
- [5] T. Kishi, S. Wakayama and S. Kohara, in *Fracture Mechanics of Ceramics* (Edited by R. C. Bradt, D. P. H. Hasselman and F. F. Lange), Vol. 8, p. 85. Plenum Press, New York (1986).
- [6] T. Nose and Fujii, *Am. Ceram. Soc.* **71**, 328 (1988).
- [7] Y. Kanto and G. Yagawa, *J. Soc. Mater. Sci. Japan* **35**, 854 (1986).
- [8] M. Enoki and T. Kishi, *Int. J. Fracture* **38**, 295 (1988).
- [9] J. F. Kalthoff, *Engng Fracture Mech.* **23**, 289 (1986).
- [10] A. G. Evans and Y. Fu, *Acta Metall.* **33**, 1525 (1985).